FORSCHUNGSZENTRUM
ROSSENDORF e.V.

FZR

FZR-60
November 1994
Preprint

E. Sobeslavsky, F.-M. Dittes and I. Rotter

Resonance phenomena at high level density

Forschungszentrum Rossendorf e.V.
Postfach 51 01 19 · D-01314 Dresden
Bundesrepublik Deutschland
Telefon (0351) 591 3657
Telefax (0351) 591 3700

Resonance phenomena at high level density

E. SOBESLAVSKY[1], F.-M. DITTES[1] AND I. ROTTER[1,2]

[1] *Forschungszentrum Rossendorf, Institut für Kern- und Hadronenphysik, D-01314 Dresden*
[2] *Technische Universität Dresden, Institut für Theoretische Physik, D-01062 Dresden*

Abstract

We investigate the behaviour of resonances as a function of the coupling strength between bound and unbound states on the basis of a simple S-matrix model. Resonance energies and widths are calculated for well isolated, overlapping and strongly overlapping resonance states. The formation of shorter and longer time scales (trapping effect) is traced. We illustrate that the cross section results from an interference of all resonance states in spite of the fact that their lifetimes may be very different.

1 Introduction

High-resolution investigations of resonance phenomena in chemical, atomic and nuclear systems became possible in recent years. They require an adequate theoretical treatment of the individual resonance states since it is insufficient, generally, to calculate average values of, e.g., the widths.

As an example, intensive experimental investigations of the large angle heavy-ion scattering have shown [1] that the standard nuclear reaction theory fails in describing the data due to the very complex reaction mechanism. The presence in the excitation functions of both narrow and broad structures indicates that there is an interplay of various reaction times, ranging from the lifetime of the compound nucleus to the time associated with shape resonances in the ion-ion potential. As a conclusion, the authors of [1] state, *a challenging problem is the development of a reaction theory which encompasses simultaneously both shorter and longer time scales so that gross, intermediate and/or fine structures and the gradual dissolution of one into the other can be quantitatively described.*

Much effort has been devoted to the theoretical investigation of the resonance phenomena at high level density [2] - [16]. The main result is the following: When the

resonances start to overlap, a redistribution of the spectroscopic values takes place. The widths of a few resonance states increase while the widths of the remaining ones desrease. The resulting separation of different time scales may amount up to more than one order of magnitude. This so-called trapping effect is observed in the frame of different models and in different many-particle systems such as nuclei and molecules. In these theoretical investigations gross, intermediate and fine structures and the gradual dissolution of one into the other can be traced.

The trapping effect occurs hierarchically [12]. In nuclear physics, this phenomenon is described by the doorway picture. A similar mechanism is discussed recently in quantum chemistry [15], [16]. This situation corresponds to the most complicated one, in which long-lived and short-lived resonances appear and the interferences between them cannot be neglected.

It is the aim of the present paper to investigate the S-matrix landscape and the corresponding Argand diagrams together with the cross section as a function of the coupling strength α between bound and unbound states. The coupling strength α determines the degree of resonance overlapping. The S-matrix landscape obtained in our calculations shows very clearly the formation of different time scales beyond a critical value $\alpha = \alpha_{crit}$. At $\alpha \gg \alpha_{crit}$ the short-lived resonances are seen in low resolution experiments while the long-lived ones do give almost no contribution to the cross section. In contrast to this, the long-lived resonances are relevant in high resolution experiments where they appear on the background of the short-lived resonances. At $\alpha \approx \alpha_{crit}$, short-lived and long-lived resonances appear simultaneously.

In Sect. 2 of the present paper, the model is sketched while the numerical results obtained are presented in Sect. 3 and discussed in Sect. 4. Some conclusions are drawn in the last section.

2 Model calculations

The model used is described e.g. in [17]. For convention, it will be outlined here.

We are going to investigate a system of N bound states coupled to a set of Λ open reaction channels. The total Hamiltonian of the system looks like

$$\mathcal{H} = \sum_{i,j=1}^{N} \mid \Psi_i\rangle H_{ij} \langle \Psi_j \mid + \sum_{c=1}^{\Lambda} \int d\varepsilon \mid \chi_c(\varepsilon)\rangle \varepsilon \langle \chi_c(\varepsilon) \mid +$$

$$\sum_{c=1}^{\Lambda}\sum_{i=1}^{N}\int d\varepsilon(\mid \Psi_i\rangle V_i^c(\varepsilon)\langle\chi_c(\varepsilon)\mid + h.c.), \tag{1}$$

where $\mid \Psi_i\rangle, i = 1,...,N, N \gg 1$, are the wave functions of the N bound states, $\mid \chi_c\rangle, c = 1,...,\Lambda, \Lambda \ll N$, denote the wave functions of Λ decay channels coupled to the bound states by an interaction V^c with components

$$V_i^c(\varepsilon) = \langle\Psi_i \mid \sqrt{\alpha}\widehat{V} \mid \chi_c(\varepsilon)\rangle,\ i = 1,...,N,\ c = 1,...,\Lambda. \tag{2}$$

The coupling vectors $V^c \equiv [V_i^c]_{i=1,...,N}$ are supposed to be pairwise orthogonal, so we neglect direct (fast) reactions. The average value of the coupling matrix element

$$\overline{\mid V_i^c \mid^2} = \frac{1}{N\cdot\Lambda}\cdot\alpha\cdot\sum_{i=1}^{N}\sum_{c=1}^{\Lambda}\mid\langle\Psi_i\mid\widehat{V}\mid\chi_c(\varepsilon)\rangle\mid^2, \tag{3}$$

is a measure of the coupling strength to the corresponding channel. Here, ε is the energy of the system.

In the following, we restrict ourselves to a finite energy region where the vectors V^c may be considered as energy-independent. Further, we restrict ourselves to time reversible systems. In this case both, H_{ij} and V^c , are real.

We choose the $N \times N$ matrix H by drawing the matrix elements randomly from a Gaussian distribution with

$$\overline{H}_{ij} = 0,\ \overline{H_{ij}^2} = \frac{1+\delta_{ij}}{N}. \tag{4}$$

For large N the spectrum is confined to the energy region $\mid E \mid \leq 2MeV$.

Analogously, the coupling vectors V^c are drawn from a Gaussian with mean value zero and variance $\langle(V_i^c)^2\rangle = \alpha$.

The scattering matrix $S_{ab}, a, b = 1,...,\Lambda$, corresponding to the Hamiltonian (1) looks as [17, 7]

$$S_{ab}(E) = \delta_{ab} - 2\pi i\sum_{i,j=1}^{N}V_i^a D_{ij}^{-1}(E)V_j^b, \tag{5}$$

where

$$D_{ij}(E) = E\delta_{ij} - H_{ij} + i\pi\sum_{c=1}^{\Lambda}V_i^c V_j^c. \tag{6}$$

Eqs. (5),(6) allow us to find the S-matrix poles as the complex eigenvalues, $E_i - \frac{1}{2}i\Gamma_i$, of an effective Hamiltonian.

$$H_{ij}^{eff}\Phi_j = \left(H_{ij} - i\pi \sum_{c=1}^{\Lambda} V_i^c V_j^c\right)\Phi_j. \tag{7}$$

From these poles, the energies, E_i, and widths, Γ_i, of the resonances are found. It is just equation(7) that is numerically treated in the present paper for a randomly choosen set of H_{ij} and V_i^c,V_j^c .

Finally, we have to emphasize that the model used works far from thresholds. It starts with N resonances states and neglects the direct reaction part as well as channel-channel coupling.

3 Results

We have calculated the widths of the resonant states, the landscapes of $\mid S_{1n}(E) \mid, n = 1,2,3$, in the complex energy plane (i.e. the lines of equal values of $\mid S_{1n}(E) \mid$ in the $(Re(E), Im(E))$ - plane), the elastic and inelastic cross sections $\sigma_{1n} = \mid \delta_{1n} - S_{1n}(E) \mid^2, n = 1,2,3,$ and Argand diagrams for $N = 16$ resonance states and $\Lambda = 3$ channels (the Argand diagrams being the energy dependent location of the S-matrix values in the (ReS_{1n}, ImS_{1n}) - plane, where only the real energy axis is regarded, i.e. $Im(E) = 0$). The coupling strength α is varied between $\alpha = 0.002$ and $\alpha = 2.000$. This corresponds to a $\overline{\Gamma}/\overline{d} \approx 0.15$ to $\overline{\Gamma}/\overline{d} \approx 200$ (where $\overline{\Gamma}$, $\overline{d}$ denote the average resonance widths and distances, respectively), so covering an area from well isolated to strongly overlapping resonances, see table 1.

In fig. 1 we have shown all $\Gamma_i(\alpha), i = 1, ..., N$, in order to illustrate the critical value $\alpha = \alpha_{crit}$ around which the redistribution of resonance widths takes place.

In the left part of fig. 2, the motion of the poles of S_{11} can be seen from the $\mid S_{11}(E) \mid$-landscapes, while in the middle the cross section is represented and in the right part the Argand diagrams. A significant absorption into other channels can be seen, $\mid S_{11}(E) \mid < 1$. Note that for all regarded cases S_{11} in the Argand diagrams moves counterclockwise with growing energies.

As long as the coupling strength α is small, $\alpha = 0.002$, all the poles of the S-matrix are close to the real energy axis (fig. 2a). This region is enlarged represented in fig. 3a.

The phase, δ, of S_{11}, $\delta = \arctan\left(\frac{Im(S_{11}(E))}{Re(S_{11}(E))}\right)$, is concentrated near $\delta = 0$ (see the right

Table 1: Mean degree of overlap $\overline{\Gamma}/\overline{d}$ of all (second column) and all but the three broadest resonances (third column) as a function of α

α	$\overline{\Gamma}/\overline{d}$	$\overline{\Gamma}_n/\overline{d}$
0.002	0.15	0.12
0.010	0.77	0.51
0.015	1.20	0.66
0.020	1.63	0.75
0.100	10.20	0.70
2.000	202.54	0.04

column of fig.(2). The Argand diagram makes a circle-like move in the vicinity of resonance energies. In correspondence to this, the cross section, σ , shows almost isolated resonances.

At $\alpha = 0.010$ (fig. 2b), $\alpha = 0.015$ (fig. 2c), $\alpha = 0.020$ (fig. 2d) three poles are separating from the other ones. The remaining 13 poles can be identified with a proper energy resolution. The cross section, σ_{11}, does not longer show well isolated resonances. The Argand diagram occupies the whole space allowed due to the unitarity of the S-matrix. The slopes and kinks correspond to energies, where a broad resonance passes (in $Re(E)$) near a narrow one (e.g. near $E \approx 0.025$, E is in arbitrary units).

The next coupling strength, $\alpha = 0.100$ (fig. 2e) is well beyond the critical region. Here, the three broad resonances in the cross sections are clearly formed (see columns 2 and 3 of table 1, where the overlap of the narrow resonances, $\overline{\Gamma_n}/\overline{d}$, is compared to the total overlap $\overline{\Gamma}/\overline{d}$). This corresponds to the fact that $\Lambda = 3$ decay channels are open. The landscape near the real axis is shown in fig. 3b.

A further growing of the coupling strength, $\alpha = 2.000$ (fig. 2f), causes the formation of dips instead of resonances in the cross section. Three poles are well separated from the other ones (as a consequence of the small number of open decay channels $N \gg \Lambda = 3$). Their widths are much larger than the widths of the long-lived resonances near the real energy axis. The latter are shown in another scale in fig. 3c (note the smaller steps of $\mid S_{11}(E) \mid$ in the region 1.00 to 1.10). One clearly sees, that an accurate description of all resonances requires two energy resolution scales, at least in the presented theoretical treatment. For nearly all energies the phase of S_{11} is now concentrated at an argument of $\delta = \pi$ what corresponds to the formation of dips in the cross section.

The cross sections and Argand diagrams for $\alpha = 2.000$ corresponding to the inelastic channels $1 \Rightarrow 2$ and $1 \Rightarrow 3$ are shown in fig. 4. Here, the cross sections show isolated resonances and the Argand diagrams are concentrated at small $Re(S_{12}), Im(S_{12})$ and $Re(S_{13}), Im(S_{13})$, respectively. Note, that direct channel-channel coupling has been neglected in our calculations.

4 Discussion of the results

The study of Argand diagrams enables us to clarify the role of the unitarity of the S-matrix, $S^{\dagger}S = 1$, in the interference picture of the cross section in each reaction channel.

For well isolated resonances, e.g. fig. 2a , the Argand diagram represents a unit circle around the origin in the complex S_{11} -plane. So, in the regarded channel in the vicinity of the resonance energy nearly all flux is concentrated on this resonance. The interferences with other states are negligible.

A growing coupling constant α causes a stronger interference with other resonances. Near $\alpha = \alpha_{crit}$ it can no longer be neglected, cf. figs. 2b, 2c, and 2d, because an intensive exchange between resonances and different channels takes place. Here, the resonances start to overlap, cf. table 1. Intermediate and fine structures appear in the cross section.

Further growing coupling strength α causes the phase δ of S_{11} preferably to be near $\delta = \pi$, see fig. 2f. That means, the resonances appear on a large background in the elastic channel. Due to the unitarity of the S-matrix, this is possible only by formation of (isolated) dips in the cross section instead of (isolated) resonances (fig. 2f). The interference between short-lived and long-lived resonances becomes important: the averaged elastic cross section is *not larger but smaller* than the cross section caused by the short-lived states alone (for a numerical example see [18]). In the inelastic channels, resonances appear.

Regarding the landscapes of $\mid S_{11}(E) \mid$ one must state that in investigations with different resolutions, different S-matrix poles are relevant. The long-lived resonances in figs. 3b, c and the short lived ones in fig. 2e, cannot be seen simultaneously.

These results show how gross, intermediate and fine structures arise in the cross section. They can be described only if the interferences between all resonances are taken into account.

5 Conclusions

We investigated the resonance phenomena as a function of the degree of overlap simulated in our calculations by the coupling strength α between bound and unbound states. We traced the picture from a situation with well isolated resonances to that one with strongly overlapping resonances. In any case, the theoretical description encompasses simultaneously both shorter and larger time scales. Most interesting is the critical region, $\alpha_{crit} \widehat{=} 0.010$ to 0.020, corresponding to $\overline{\Gamma}/\overline{d} \approx 0.8$ to 1.6, where the separation of different time scales starts. Here, the resonances overlap and the Argand diagram has a complicated structure. The cross section results from an *interference picture* to which all resonances give a contribution.

We also investigated the separation of different types of S-matrix poles. Our model provides a good demonstration of the trapping phenomenon for the relatively low number, $N = 16$, of resonances. The results illustrate the formation of gross, intermediate and fine structures in the cross section corresponding to the existence of different time scales of the process.

The existence of a hierarchy of short and long living states is known in nuclear physics studies, e.g. in heavy ion scattering. It is, however, discussed also in many-body scattering problems of molecular physics and in problems of atomic and solid state physics, as well as in the scattering of electrons or light waves by disordered media.

Acknowledgement: Valuable discussions with W. Cassing, I. Iskra and M. Müller are greatfully acknowledged. The present investigation is supported by the Deutsche Forschungsgemeinschaft under the contract number Ro-922/1.

References

[1] P. Braun-Munzinger and J. Barrette, Phys. Rep. 87, 210 (1982)

[2] P. Kleinwächter and I. Rotter, Phys. Rev. C 32, 1742 (1985); I. Rotter, J. Phys. G 12, 1407 (1986); 14, 857 (1988); Fortschr. Phys. 36, 781 (1988)

[3] V.V. Sokolov and V.G. Zelevinsky, Phys. Lett. B 202, 10 (1988); Nucl. Phys. A 504, 562 (1989)

[4] V.B. Pavlov-Verevkin, Phys. Lett. A 129, 168 (1988); F. Remacle, M. Munster, V.B. Pavlov-Verevkin and M. Desouter-Lecomte, Phys. Lett. A 145, 265 (1990)

[5] F.-M. Dittes, W. Cassing and I. Rotter, Z. Phys. A 337, 243 (1990)

[6] I. Rotter, Rep. Prog. Phys. 54, 635 (1991) and references

[7] F.-M. Dittes, I. Rotter and T.H. Seligman, Phys. Lett. A 158, 14 (1991)

[8] F.-M. Dittes, H.L. Harney and I. Rotter, Phys. Lett. A 153, 451 (1991)

[9] V.V. Sokolov and V.G. Zelevinsky, Ann. Phys. (N.Y.) 216, 323 (1992) and references therein

[10] F. Haake, F. Izrailev, N. Lehmann, D. Saher and H.J. Sommers, Z. Phys. B 88, 359 (1992)

[11] R.D. Herzberg, P. von Brentano and I. Rotter, Nucl. Phys. A 556, 107 (1993)

[12] W. Iskra, I. Rotter and F.-M. Dittes, Phys. Rev. C 47, 1086 (1993)

[13] K. Someda, H. Nakamura and F.H. Mies, Progr. Theor. Phys. Suppl. (1994)

[14] W. Iskra, M. Müller and I. Rotter, J. Phys. G 19, 2045 (1993); G 20 (1994)

[15] S.A. Reid and H. Reisler, J. Chem. Phys., to be published

[16] V.A. Mandelshtam, H.S. Taylor, C. Jung, H.F. Bowen and D.J. Kouri, to be published

[17] C. Mahaux and H.A. Weidenmüller, *Shell Model Approach to Nuclear Reactions, Amsterdam: North-Holland, 1969*

[18] P. Kleinwächter and I. Rotter, J. Phys. G: Nucl. Phys. 12, 821 (1986)

Figure 1

The widths $\Gamma_i, i = 1, ..., N$, in dependence on the coupling strength α. The $N = 16$ bound states are distributed randomly. The calculation is performed in steps of $\Delta\alpha = 0.002$.

Figure 2

Landscape of $\mid S_{11}(E) \mid$ over the complex energy plane, the elastic coupling cross sections $\sigma_{11}(E) = \mid 1 - S_{11}(E) \mid^2$, and Argand diagrams for $N = 16$ resonances and $\Lambda = 3$ open channels for different values of the coupling constant α: **(a)** $\alpha = 0.002$, **(b)** $\alpha = 0.010$, **(c)** $\alpha = 0.015$, **(d)** $\alpha = 0.020$, **(e)** $\alpha = 0.100$, **(f)** $\alpha = 2.000$, corresponding to $\overline{\Gamma}/\overline{d} \cong 0.15$, 0.77, 1.20, 1.63, 10.20 and 202.54, respectively. The contour lines in the left column correspond to $\mid S_{11}(E) \mid = 1.0, ..., 5.0$ and are equidistant with a difference of $\Delta \mid S_{11}(E) \mid = 0.1$ for figs. a, b, c and d, while they correspond to $\mid S_{11}(E) \mid = 1.0, ..., 20.0$ with $\Delta \mid S_{11}(E) \mid = 0.5$ for fig. e and to $\mid S_{11}(E) \mid = 1.0, ..., 81.0$, $\Delta \mid S_{11}(E) \mid = 4.0$ for fig. f. Note the different $Im(E)$-scale on the left hand side of figs.

e and f!

Figure 3

Enlarged details of figs. 2a, 2e and 2f, correspondingly, showing the landscape of $\mid S_{11}(E) \mid$ near the real energy axis. Here, the contour lines correspond to $\mid S_{11}(E) \mid = 1.0, ..., 1.2, \Delta \mid S_{11}(E) \mid = 0.01$ for fig. a, and to $\mid S_{11}(E) \mid = 1.0, ..., 5.0, \Delta \mid S_{11}(E) \mid = 0.1$ for fig. b. For fig. c the contour lines run from $\mid S_{11}(E) \mid = 1.00, ..., 1.10$ with a step of $\Delta \mid S_{11}(E) \mid = 0.01$ and from $\mid S_{11}(E) \mid = 1.1, ..., 2.0$ with a step of $\Delta \mid S_{11}(E) \mid = 0.1$. Note the different $Im(E)$-scales!

Figure 4

The inelastic reaction cross sections $\sigma_{12}(E) = \mid S_{12}(E) \mid^2$ and $\sigma_{13}(E) = \mid S_{13}(E) \mid^2$, and the corresponding Argand diagrams for $N = 16$ resonances, $\Lambda = 3$ open decay channels and $\alpha = 2.000$.

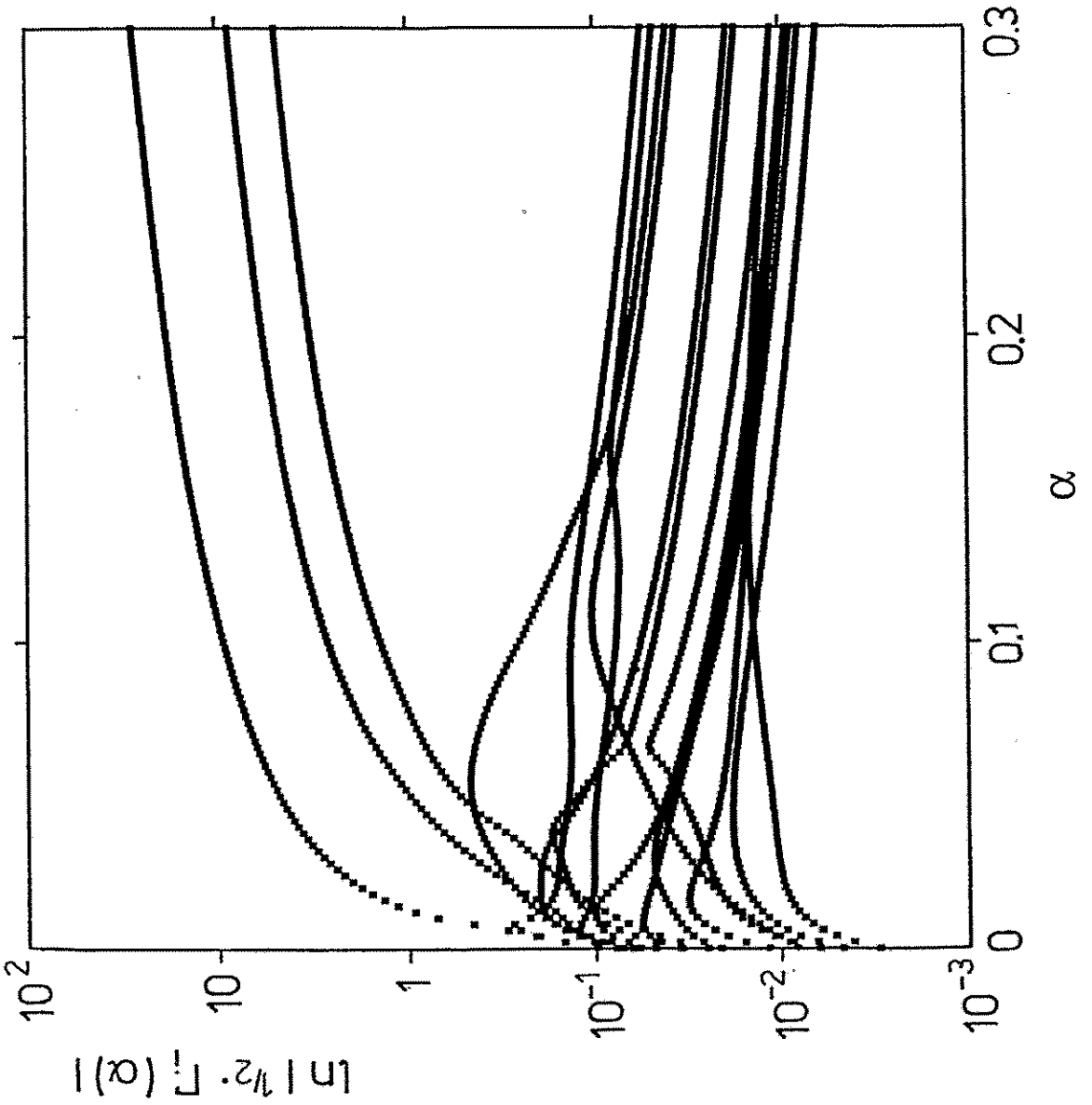

Fig.1

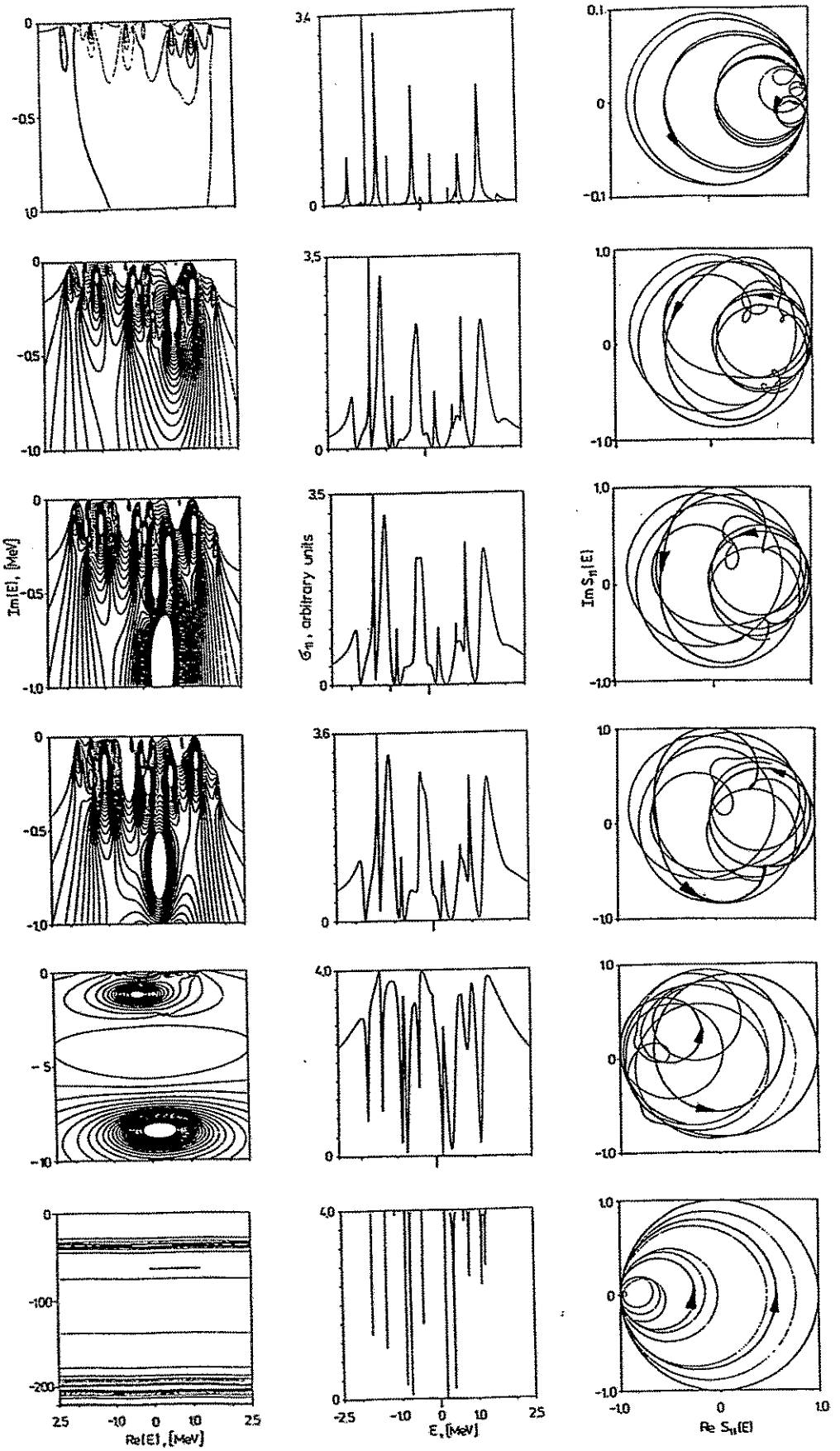
Im[E], [MeV]
σ_fi, arbitrary units
Im S_fi(E)
Re[E], [MeV]
E, [MeV]
Re S_fi(E)
(a) α = 0.002
(b) α = 0.010
(c) α = 0.015
(d) α = 0.020
(e) α = 0.100
(f) α = 2.000

Fig.2

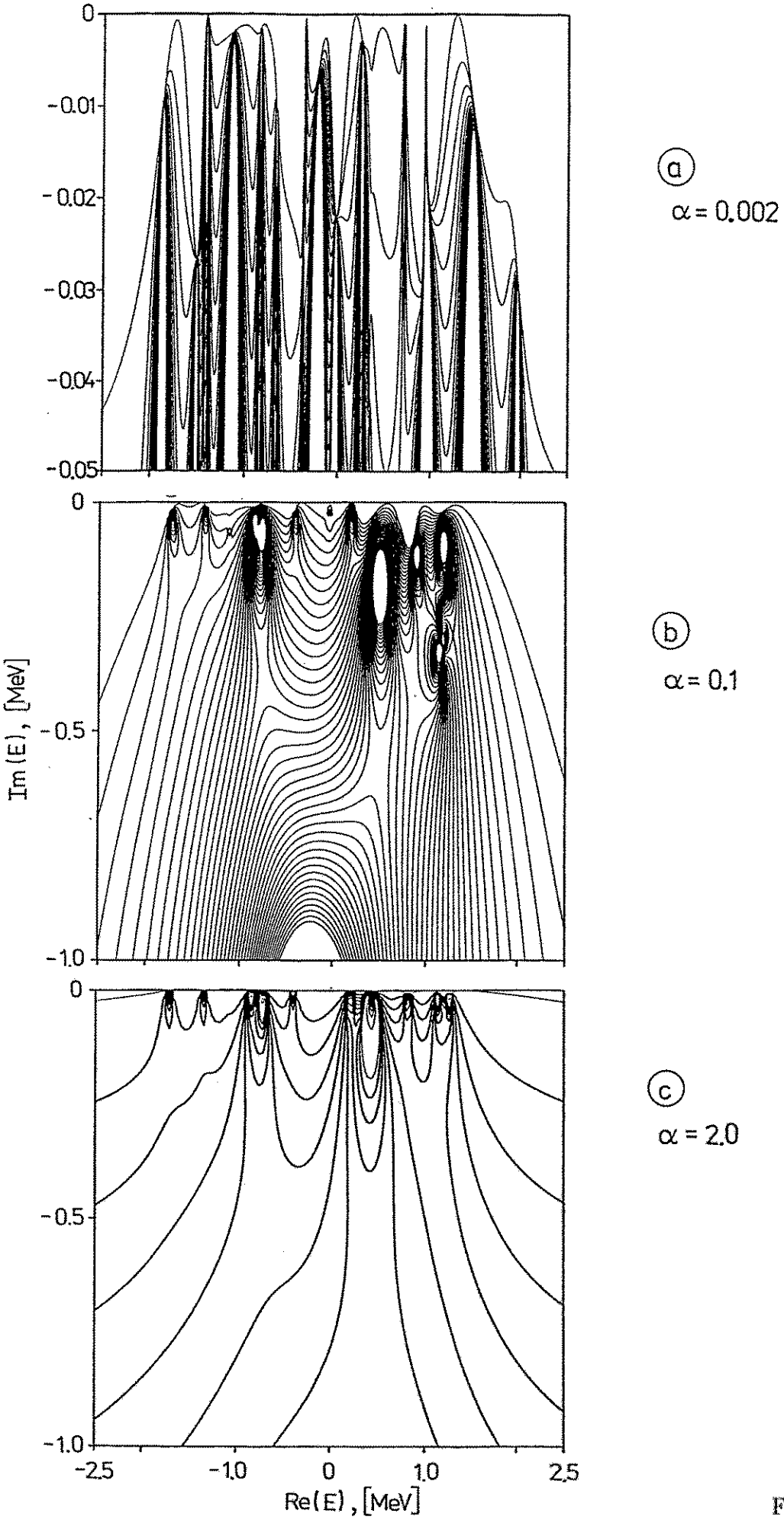
0
-0.01
-0.02
-0.03
-0.04
-0.05
a
α = 0.002
0
-0.5
-1.0
Im (E), [MeV]
b
α = 0.1
0
-0.5
-1.0
c
α = 2.0
-2.5
-1.0
0
1.0
2.5
Re(E), [MeV]

Fig.3

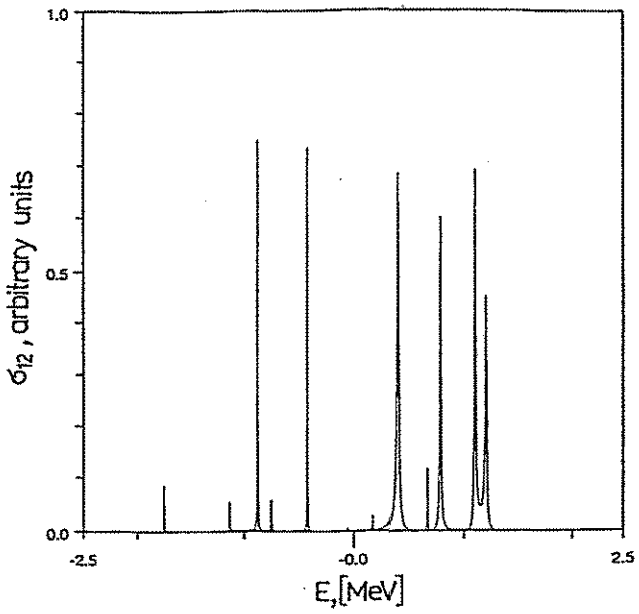
1.0
0.5
0.0
σ_{12}, arbitrary units
-2.5
-0.0
2.5
E,[MeV]

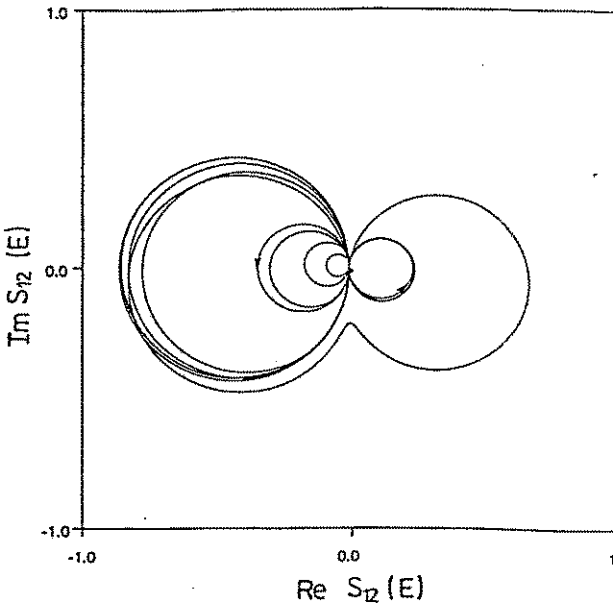
1.0
0.0
-1.0
Im S_{12} (E)
-1.0
0.0
Re S_{12} (E)

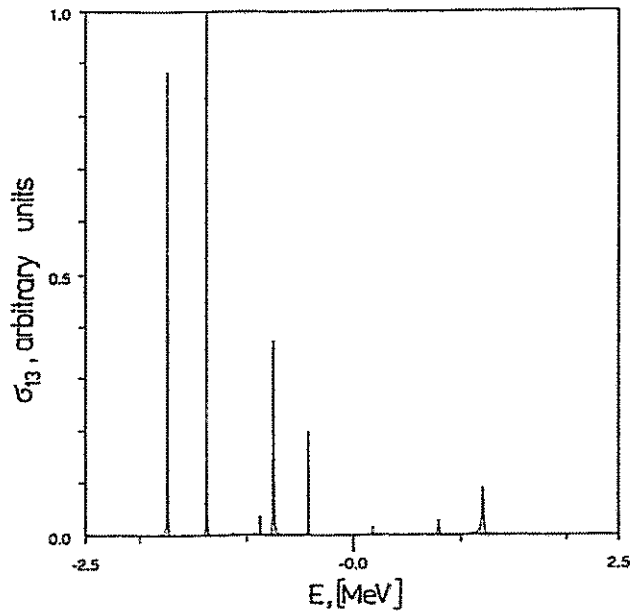
1.0
0.5
0.0
σ_{13}, arbitrary units
-2.5
-0.0
2.5
E,[MeV]

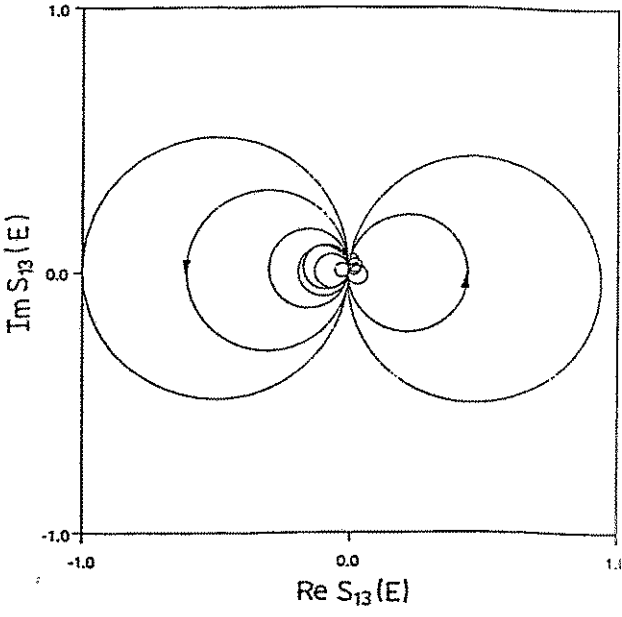
1.0
0.0
-1.0
Im S_{13} (E)
-1.0
0.0
Re S_{13} (E)

Fig.4